nature medicine

2-hydroxyglutarate detection by magnetic resonance spectroscopy in subjects with *IDH*-mutated gliomas

Changho Choi[1,2], Sandeep K Ganji[1,2], Ralph J DeBerardinis[3–5], Kimmo J Hatanpaa[5–7], Dinesh Rakheja[6,8], Zoltan Kovacs[1], Xiao-Li Yang[5,7,9], Tomoyuki Mashimo[5,7,9], Jack M Raisanen[5–7], Isaac Marin-Valencia[3], Juan M Pascual[3,10,11], Christopher J Madden[5,7,12], Bruce E Mickey[5,7,12], Craig R Malloy[1,2,9,13], Robert M Bachoo[5,7,9,10] & Elizabeth A Maher[5,7,9,10]

Mutations in isocitrate dehydrogenases 1 and 2 (*IDH1* and *IDH2*) have been shown to be present in most World Health Organization grade 2 and grade 3 gliomas in adults. These mutations are associated with the accumulation of 2-hydroxyglutarate (2HG) in the tumor. Here we report the noninvasive detection of 2HG by proton magnetic resonance spectroscopy (MRS). We developed and optimized the pulse sequence with numerical and phantom analyses for 2HG detection, and we estimated the concentrations of 2HG using spectral fitting in the tumors of 30 subjects. Detection of 2HG correlated with mutations in *IDH1* or *IDH2* and with increased levels of D-2HG by mass spectrometry of the resected tumors. Noninvasive detection of 2HG may prove to be a valuable diagnostic and prognostic biomarker.

Isocitrate dehydrogenase converts isocitrate to α-ketoglutarate (αKG) in the cytosol (IDH1) and mitochondria (IDH2). The recent identification of mutations in *IDH1* and *IDH2* among most humans with World Health Organization (WHO) grade 2 and 3 gliomas[1,2] has directed attention to the role of abnormal metabolism in the pathogenesis and progression of these primary brain tumors. The mutations are confined to the active site of the enzyme and result in a gain of function that generates 2HG (ref. 3) and induces DNA hypermethylation[4,5]. The abundance of this metabolite, normally present in vanishingly small quantities, can be elevated by orders of magnitude in gliomas with *IDH1* or *IDH2* mutations. Intracellular concentrations on the order of several micromoles per gram of tumor have been reported[3].

Although the metabolic consequences and downstream molecular effects of these mutations are yet to be elucidated, their potential value as diagnostic and prognostic markers in gliomas has been established from their clear association with improved overall survival when outcomes are compared between *IDH*-mutated and *IDH* wild-type tumors[2,6]. Immunohistochemistry with a commercially available antibody to the R132H mutation of *IDH1* identifies approximately 93% of the mutations, but the remaining 7% of tumors carrying a different *IDH1* or an *IDH2* mutation require direct sequencing for detection[7]. As 2HG is produced by all known *IDH*-mutant enzymes, evaluation of 2HG abundance is an alternative indirect method for determining *IDH* status. The finding that 2HG is present at high levels in *IDH*-mutated gliomas has raised the possibility that this metabolite could be detected noninvasively by MRS. Brain magnetic resonance imaging is the primary modality for clinical evaluation of people with gliomas, so the ability to detect 2HG by MRS could provide important diagnostic and prognostic information.

Here we report the noninvasive detection of 2HG in glioma *in vivo* by MRS at 3 tesla (T). We optimized the point-resolved spectroscopy (PRESS)[8] and difference editing[9] sequences with quantum-mechanical and phantom analyses for detection of 2HG in the human brain and applied them to tumor masses in 30 adults with all grades of gliomas. Analysis of MRS data was blinded to *IDH* status. For each case in which 2HG was detected by MRS, we confirmed an *IDH1* or *IDH2* mutation in the tumor. Failure to detect 2HG by MRS was associated with the detection of wild-type *IDH1* and *IDH2* in each case. The sensitivity and specificity of the method described here and the ease with which it could be incorporated into standard magnetic resonance imaging suggests that 2HG detection by MRS may be an important biomarker in the clinical management of these patients.

RESULTS

Optimization of MRS methods

A 2HG molecule has five nonexchangeable scalar-coupled protons, resonating at 4.02 p.p.m., 2.27 p.p.m., 2.22 p.p.m., 1.98 p.p.m. and 1.83 p.p.m.[10], giving rise to multiplets at approximately three locations at 3 T; that is, 4.02 p.p.m. (H2), ~2.25 p.p.m. (H4 and H4′) and ~1.9 p.p.m.

[1]Advanced Imaging Research Center, University of Texas Southwestern Medical Center, Dallas, Texas, USA. [2]Department of Radiology, University of Texas Southwestern Medical Center, Dallas, Texas, USA. [3]Department of Pediatrics, University of Texas Southwestern Medical Center, Dallas, Texas, USA. [4]McDermott Center for Human Growth and Development, University of Texas Southwestern Medical Center, Dallas, Texas, USA. [5]Harold C. Simmons Cancer Center, University of Texas Southwestern Medical Center, Dallas, Texas, USA. [6]Department of Pathology, University of Texas Southwestern Medical Center, Dallas, Texas, USA. [7]Annette Strauss Center for Neuro-Oncology, University of Texas Southwestern Medical Center, Dallas, Texas, USA. [8]Children's Medical Center, Dallas, Texas, USA. [9]Department of Internal Medicine, University of Texas Southwestern Medical Center, Dallas, Texas, USA. [10]Department of Neurology and Neurotherapeutics, University of Texas Southwestern Medical Center, Dallas, Texas, USA. [11]Department of Physiology, University of Texas Southwestern Medical Center, Dallas, Texas, USA. [12]Department of Neurological Surgery, University of Texas Southwestern Medical Center, Dallas, Texas, USA. [13]Veterans Affairs North Texas Health Care System, Dallas, Texas, USA. Correspondence should be addressed to C.C. (changho.choi@utsouthwestern.edu) or E.A.M. (elizabeth.maher@utsouthwestern.edu).

Received 26 April 2011; accepted 17 August 2011; published online 26 January 2012; corrected online 31 January 2012 (details online); doi:10.1038/nm.2682

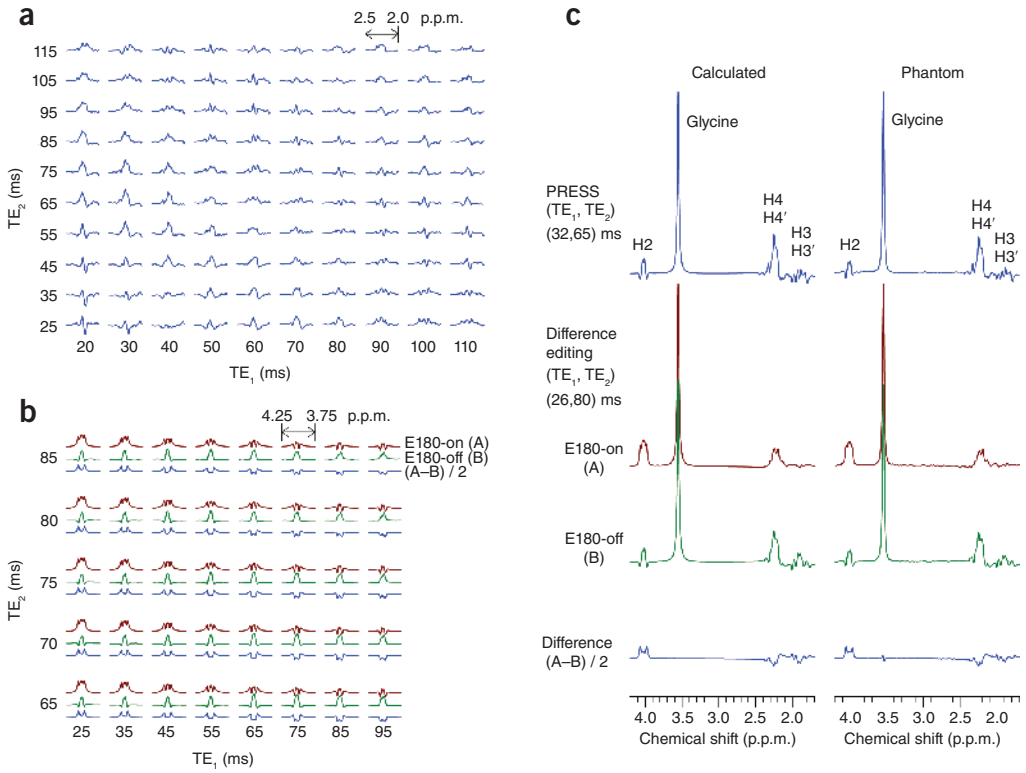

Figure 1 Theoretical and experimental spectra of 2HG. (**a**) Quantum-mechanically calculated spectra of the 2HG H4 resonances, at 3 T, are plotted against TE_1 and TE_2 of PRESS (subecho times of the first slice– and second slice–selective 180° radiofrequency pulses, respectively). (**b**) Calculated difference-edited multiplets of the 2HG H2 resonance are plotted against subecho times TE_1 and TE_2 of scalar difference editing. Shown for each TE_1-TE_2 pair are, top to bottom, E180-on (brown) and E180-off (green) subspectra, and the difference between the two subspectra (blue). Here, E180 denotes editing 180° pulses tuned to 1.9 p.p.m. PRESS and edited spectra are all broadened to a singlet line width of 4 Hz. Spectra in **a** and **b** are scaled equally for direct comparison. Relaxation effects were not included in the calculations. (**c**) Calculated and phantom spectra of 2HG for PRESS and difference editing. The echo times were 97 ms and 106 ms for PRESS and editing. The concentrations of 2HG and glycine in the phantom were both 10 mM (pH = 7.0). Spectra are scaled with respect to the glycine singlet at 3.55 p.p.m.

(H3 and H3′) (**Supplementary Fig. 1**). The 2HG resonances are all scalar coupled, and, consequently, the spectral pattern and signal strength vary with changing echo time of MRS sequence. A maximum 2HG signal may be expected at ~2.25 p.p.m. where the H4 and H4′ spins resonate proximately to each other. Because of its capability of full refocusing, in the present study we used a PRESS sequence as a major tool for 2HG measurement.

We conducted quantum mechanical simulations to search for optimal experimental parameters. The simulation indicated that the 2HG H4 resonances give rise to a maximum multiplet at total echo time of 90–100 ms, for which the first subecho time, TE_1, is shorter than the second subecho time, TE_2 (**Fig. 1a**). Given the large spectral distance of the H2 resonance from its weak coupling partners (H3 spins), we also measured the H2 resonance by means of difference editing. Selective 180° rotation of the H3 spins was switched on and off within a PRESS sequence in alternate scans to induce unequal H2 multiplets in subspectra. Subtraction between the spectra generated an edited 2HG H2 multiplet, canceling other resonances that were not affected by the editing 180° pulses. The computer simulation indicated that a large edited H2 signal can be obtained using a short-echo-time set in which TE_1 should be the shortest possible (**Fig. 1b**). We optimized the subecho times of the PRESS and difference editing sequences to (TE_1, TE_2) = (32, 65) ms and (26, 80) ms, respectively. We tested these optimized MRS sequences in an aqueous solution with 2HG that was synthesized in house. The spectral pattern and signal intensity of 2HG were consistent between calculation and experiment (**Fig. 1c**).

The optimized PRESS provided a 2HG multiplet at approximately 2.25 p.p.m. with maximum amplitude among echo times greater than 40 ms (**Supplementary Fig. 2a**,**b**). Moreover, the optimized echo time gave rise to narrowing of the multiplet and substantial reduction of 2HG signals at approximately 1.9 p.p.m. Similar signal modulation occurred in the glutamate multiplets, allowing 2HG to be measured with high selectivity against the background signals of adjacent resonances (**Supplementary Fig. 2c**,**d**). The optimized echo time is relatively long, so signal loss due to transverse relaxation effects may be considerable *in vivo*. However, given that 2HG does not have a well-defined spectral pattern at short echo times (for example, 30 ms), the 2HG signals can be better resolved at the optimized long echo time, benefiting from the suppressed complex baseline signals of macromolecules. The signal yield of 2HG in difference editing was low (38%) compared to that in PRESS (**Fig. 1**), but the editing provides a useful tool for proving 2HG elevation because the edited signal at 4.02 p.p.m. is uniquely generated via the coupling connections of 2HG. *In vivo*, because the difference editing uses spectral difference induced by selective 180° rotations tuned at approximately 1.9 p.p.m., the 4.15-p.p.m. resonance of the glutamate moiety of N-acetylaspartylglutamate[11] is co-edited, but the resonance is relatively distant from the 2HG 4.02-p.p.m. resonance and thus does not interfere with 2HG editing (**Supplementary Fig. 3**). The lactate resonance at 4.1 p.p.m.[12] is not co-edited because the coupling partners at 1.31 p.p.m. are not influenced by the editing 180° pulse.

For spectral fitting, in the present study we used model spectra that were calculated including the effects of the volume-localized radiofrequency pulses used for *in vivo* measurements, allowing spectral fitting by signal patterns identical to those obtained by experiment. Calculation of spectra at numerous echo times for MRS sequence optimization was efficiently accomplished using the product operator-based transformation-matrix algorithm in the quantum-mechanical simulations[13–15] (**Supplementary Methods**). The spectral pattern of 2HG is pH dependent[10], with large shifts noted for pH < 6 (**Supplementary Fig. 4**). We performed computer simulations and MRS sequence optimization for 2HG detection assuming pH ~7.0 in tumors[16–18].

Table 1 Correlation between 2HG detection by MRS PRESS and *IDH1* and *IDH2* mutational status

Histological diagnosis	2HG by MRS (mM (CRLB))	*IDH1* and *IDH2* mutations by DNA sequencing	*IDH1* R132H by immunohistochemistry
Oligodendroglioma (WHO grade 2)	2.7 (13%)	*IDH2* (R172K)	Negative
Oligodendroglioma (WHO grade 2)	3.3 (11%)	*IDH1* (R132H)	Positive
Oligodendroglioma (WHO grade 2)	2.6 (14%)	*IDH1* (R132C)	Negative
Oligodendroglioma (WHO grade 2)	1.7 (17%)	*IDH1* (R132H)	Positive
Oligodendroglioma (WHO grade 2)	3.3 (7%)	*IDH1* (R132C)	Negative
Astrocytoma (WHO grade 2)	4.2 (10%)	*IDH1* (R132H)	Positive
Astrocytoma (WHO grade 3)	2.1 (16%)	*IDH1* (R132H)	Positive
Oligoastrocytoma (WHO grade 3)	3.9 (6%)	*IDH1* (R132H)	Positive
Oligodendroglioma (WHO grade 3)	8.9 (3%)	*IDH1* (R132H)	Positive
Oligoastrocytoma (WHO grade 3)	3.4 (8%)	*IDH2* (R172W)	Negative
Astrocytoma (WHO grade 3)	2.7 (11%)	*IDH2* (R172G)	Negative
Astrocytoma (WHO grade 3)	5.3 (6%)	*IDH1* (R132H)	Positive
Astrocytoma (WHO grade 3)	2.5 (16%)	*IDH1* (R132C)	Negative
Astrocytoma (WHO grade 3)	2.2 (15%)	*IDH1* (R132C)	Negative
Astrocytoma (WHO grade 3)	ND	None	Negative
Secondary glioblastoma (WHO grade 4)	2.1 (15%)	*IDH1* (R132H)	Positive
Glioblastoma (WHO grade 4)	ND	None	Negative
Glioblastoma (WHO grade 4)	ND	None	Negative
Glioblastoma (WHO grade 4)	ND	None	Negative
Glioblastoma (WHO grade 4)	ND	None	Negative
Glioblastoma (WHO grade 4)	ND	None	Negative
Glioblastoma (WHO grade 4)	ND	None	Negative
Glioblastoma (WHO grade 4)	ND	None	Negative
Glioblastoma (WHO grade 4)	ND	None	Negative
Glioblastoma (WHO grade 4)	ND	None	Negative
Glioblastoma (WHO grade 4)	ND	None	Negative
Glioblastoma (WHO grade 4)	ND	None	Negative
Glioblastoma (WHO grade 4)	ND	None	Negative
Glioblastoma (WHO grade 4)	ND	None	Negative

The MRS measures labeled 'ND' (not detected) were 2HG estimates ≤0.08 mM with CRLB ≥85%. The MRS estimates of 2HG concentrations were significantly different between mutated and wild-type *IDH* ($P = 6 \times 10^{-8}$, unpaired *t*-test).

2HG detected in MRS spectra from subjects with gliomas

We included 30 subjects with gliomas in the 2HG MRS analysis (**Table 1**). The optimized PRESS was applied to the tumor mass. A representative normal brain spectrum (**Fig. 2a**) showed the expected pattern of choline, creatine and *N*-acetylaspartate (NAA) without evidence of 2HG. In contrast, the classic pattern of elevated choline with decreased creatine and NAA was present in all glioma grades (**Fig. 2b–f**). A signal attributed to 2HG was discernible at 2.25 p.p.m. in the WHO grade 2 and 3 tumors (**Fig. 2c–f**), but not in the glioblastoma (**Fig. 2b**). We identified an *IDH1* or *IDH2* mutation in each of these cases. We analyzed the single-voxel–localized PRESS data with linear combination of model (LCModel) software[19], using spectra of 20 metabolites as basis sets, calculated incorporating the volume-localized pulses. We estimated the concentration of 2HG using the brain water signal from the voxel as reference and adjusted the relaxation effects on the observed metabolite signals using published relaxation times of brain metabolites for 3 T[20–22]. With a 2-min scan on $2 \times 2 \times 2$ cm^3 areas of brain tissue, 2HG was measurable for concentrations >1.5 mM, with Cramér-Rao lower bound (CRLB) < 18% (**Table 1**). With the use of precisely calculated model spectra for spectral fitting, the LCModel fits reproduced the *in vivo* spectra closely, resulting in residuals at the noise levels that did not show considerable chemical-shift dependences.

γ-Aminobutyric acid (GABA), glutamate and glutamine have resonances of 2.1–2.4 p.p.m. Thus, the signals are partially overlapped with the 2HG 2.25-p.p.m. signal in PRESS spectra and can interfere with 2HG estimation depending on their signal strengths. Spectral fitting with the calculated spectra enabled resolution of the metabolites with CRLB < 20% for concentrations above ~2 mM (**Fig. 2**). We validated the PRESS detection of 2HG using two methods. First, we compared spectral fitting outputs from a basis set with or without a 2HG signal. For spectra without measurable 2HG signals (**Fig. 3a**), the residuals were essentially identical between the two fitting methods. However, spectra with a noticeable signal at 2.25 p.p.m., when fitted using a basis set without 2HG, resulted in large residuals at 2.25 p.p.m. (**Fig. 3a**). For spectra with intermediate 2HG concentrations, the residuals were progressively larger with increasing 2HG estimates. This result shows that the signal at 2.25 p.p.m. is primarily attributable to 2HG without substantial interference from the neighboring resonances. Second, we used difference editing to confirm the PRESS measurements of 2HG in seven subjects. When a signal at 2.25 p.p.m. was discernible in PRESS spectra, we detected an edited H2 signal at 4.02 p.p.m. (**Fig. 3b**). When 2HG was not measurable in PRESS spectra, there was no observable edited peak at 4.02 p.p.m. (**Fig. 3b**). This co-detection of the PRESS 2.25 p.p.m. peak and the edited 4.02 p.p.m. signal supports the idea that the signals are both attributable to 2HG. The similarity between the 2HG concentrations

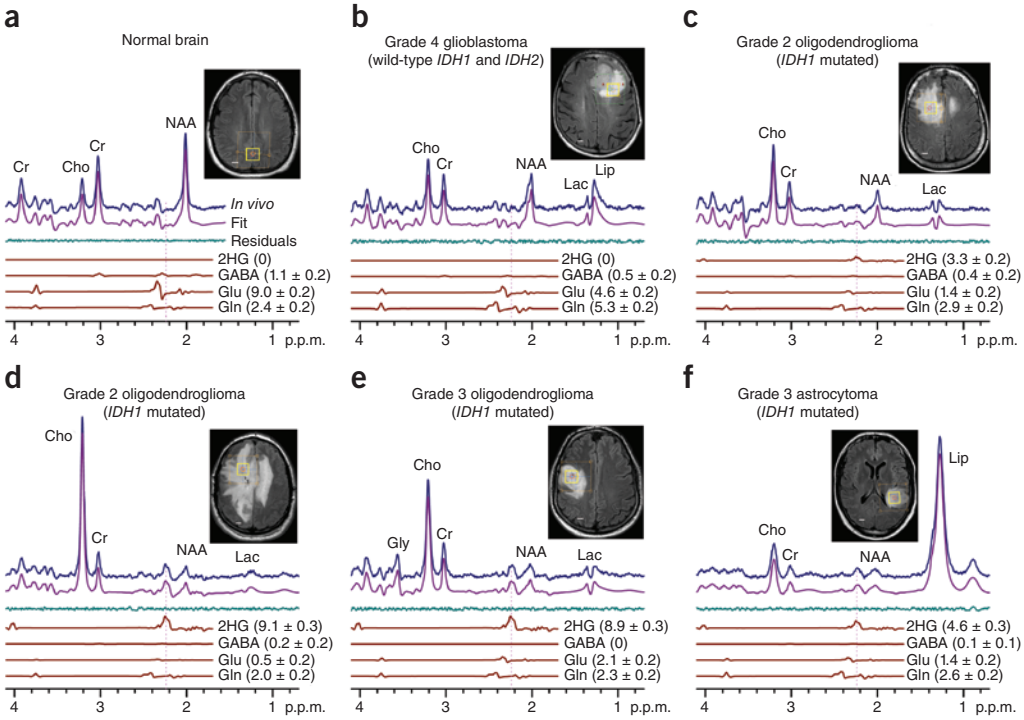

Figure 2 *In vivo* ^{1}H spectra and analysis. (**a**–**f**) *In vivo* single-voxel–localized PRESS spectra from normal brain (**a**) and tumors (**b**–**f**), at 3 T, are shown together with spectral fits (LCModel) and the components of 2HG, GABA, glutamate and glutamine, as well as voxel positioning ($2 \times 2 \times 2$ cm^3). Spectra are scaled with respect to the water signal from the voxel. Vertical lines are drawn at 2.25 p.p.m. to indicate the H4 multiplet of 2HG. Shown in brackets is the estimated metabolite concentration (mM) ± s.d. Cho, choline; Cr, creatine; Glu, glutamate; Gln, glutamine; Gly, glycine; Lac, lactate; Lip, lipids. Scale bars, 1 cm.

estimated by PRESS and editing provides evidence that the PRESS measurement of 2HG is valid, as the edited 2HG signal at 4.02 p.p.m. was generated without substantial interference from the scalar coupling connection between the 4.02 p.p.m. and ~1.9 p.p.m. resonances, which is a unique feature of 2HG among known brain metabolites[12].

Validation of MRS measures of 2HG by tissue analysis

We analyzed each tumor for *IDH* gene status by immunohistochemistry for the IDH1 R132H mutation and by gene sequencing of *IDH1* and *IDH2* (**Table 1**). Of the 30 subjects studied, 15 had measurable 2HG by MRS, and in each case we confirmed an *IDH1* (12 of 15 subjects) or an *IDH2* (3 of 15 subjects) mutation. The remaining 15 subjects did not have detectable 2HG by MRS (≤0.08 mM, CRLB > 85%), and analysis of *IDH1* and *IDH2* revealed no mutations. The MRS estimates of 2HG concentrations were significantly different between subjects with *IDH* mutations and wild-type *IDH* genes (unpaired *t*-test; $P = 6 \times 10^{-8}$).

We validated these results further by measuring D-2HG and L-2HG concentrations in tumor samples by liquid chromatography–tandem mass spectrometry (LC-MS/MS) for the 13 subjects for whom sufficient frozen material from the initial tumor resection was available (**Supplementary Table 1**). Samples from the brain tissue adjacent to tumors were available for analysis from three subjects; thus, this tissue served as relative normal controls (**Supplementary Fig. 5**). L-2HG and D-2HG were clearly differentiated in the spectra. Five wild-type *IDH1* and *IDH2* glioblastoma tumors had similar concentrations of L-2HG and D-2HG. In all tumor samples, L-2HG was <1.0 nmol per mg protein. In marked contrast, D-2HG levels in *IDH1*- and *IDH2*-mutated tumors were 20-fold to 2,000-fold higher than those in wild-type *IDH* glioblastomas (**Supplementary Fig. 6**). Taken together, these data show that the presence of a 2HG peak in MRS is 100% correlated with the presence of a mutation in *IDH1* or *IDH2* and elevated concentrations of D-2HG in the tumor. Moreover, the absence of a 2HG peak when MRS is performed in a tumor mass is 100% correlated with wild-type *IDH1* and *IDH2* and lack of accumulation of D-2HG in the tumor tissue. Thus, the ability to detect 2HG by MRS in a tumor mass is both highly sensitive and specific.

Development of multivoxel imaging of 2HG

We extended the optimized PRESS echo time method to multivoxel imaging of 2HG. The subject with grade 3 oligodendroglioma, whose single-voxel MRS data are shown in **Figure 2e**, was scanned with 1×1 cm^2 resolution on a slice 1.5 cm thick that included the tumor mass (**Fig. 4a**). The patterns of the single voxel–acquired spectra were reproduced in spectra obtained with the multi-voxel MRS method. The 2HG signal at 2.25 p.p.m. was clearly discernible in spectra from the tumor regions (**Fig. 4b**). Spectra from contralateral normal brain showed no 2HG signals at 2.25 p.p.m. (**Fig. 4c**). A map of 2HG concentrations (**Fig. 4d**) showed that 2HG was concentrated at the center of the T_2w-FLAIR hyperintensity region. We estimated the 2HG concentrations using the normal brain NAA concentration of 12 mM[12] as reference, giving a 2HG concentration approximately 9 mM at the center of the tumor mass, in agreement with the 2HG estimates by single-voxel MRS. The spatial distribution pattern of choline was similar to that of 2HG in the region of T_2w-FLAIR hyperintensity but, as expected, was found throughout the brain, whereas 2HG showed rapid drop off in normal brain. The NAA concentrations were low in the tumor mass, and the choline/NAA ratio in tumors was high relative to that of normal brain tissue. Because of their ability to detect 2HG in small volumes, the metabolic measures by the multivoxel MRS method may contain reduced partial-volume effects compared to the single-voxel MRS. As 2HG is unique to tumor cells, the specificity of detection is a key advance in clinical MRS for *IDH*-mutated gliomas.

DISCUSSION

We have detected 2HG noninvasively by optimized MRS methods in subjects with gliomas and have shown concordance of 2HG levels with mutations in *IDH1* and *IDH2*, as well as accumulation of 2HG in tumor tissue. To our knowledge, this is currently the only direct metabolic consequence of a genetic mutation in a cancer cell that can be identified through noninvasive imaging. The signal overlaps of 2HG with GABA, glutamate and glutamine, which occur in short-echo-time standard data acquisitions, were overcome with multiplet narrowing by MRS sequence optimization and spectral fitting using precisely

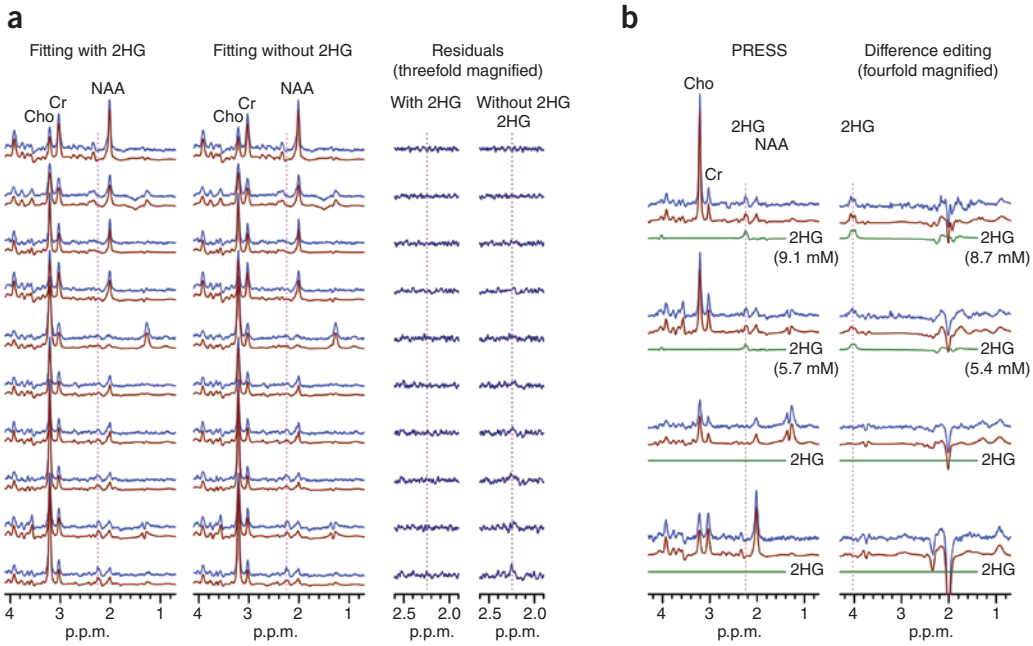

Figure 3 Validation of 2HG PRESS measurements. (**a**) LCModel fitting results (fits and residuals) of PRESS spectra obtained with basis set with or without 2HG. Data are displayed in order of increasing 2HG estimates, above to below. (**b**) PRESS and difference-edited spectra from four subjects are shown in pairs, together with LCModel fits and 2HG signal components. Vertical lines are drawn at 2.25 p.p.m. and 4.02 p.p.m. in the PRESS and edited spectra, respectively.

calculated basis spectra of metabolites. The methods presented here estimated metabolite concentrations using the brain water signal as reference in tumors, assuming an equal contribution of gray and white matter. The metabolite estimation may be valid only when the water concentration is similar among regions of the brain and between normal brain and tumor tissues. The water concentration in tumors could be increased as a result of the effects of high cellularity or brain edema, which would result in an underestimate of metabolite concentrations in the present study. Given a maximum possible water concentration of 55.6 M (bulk water), the true metabolite concentrations could be up to 30% higher than our estimates, which were obtained using a water concentration of 42.3 M, calculated from the published values for the water concentrations in gray and white matter[23]. Although uncertainties in metabolite estimates can theoretically be minimized by using an external reference signal such as from a phantom[24], referencing with respect to brain water signals may be a realistic means of estimating metabolite concentrations in tumors[25].

Two studies have previously reported *in vivo* detection of 2HG in the brains of people with 2-hydroxyglutaric aciduria[26,27]. Large singlet-like signals at 2.5–2.6 p.p.m. were assigned to 2HG, although this chemical shift assignment is not consistent with *in vitro* high-resolution magnetic resonance spectra of 2HG at neutral pH[10]. A 2HG signal at approximately 2.5 p.p.m., which is actually a multiplet, can occur only at low pH (~2.5), as reported previously[10] and confirmed in this work (**Supplementary Fig. 4**). The pH measured noninvasively in a wide range of tumors ranges between 6.8 and 7.2. Even using microelectrode studies, the lowest pH measured was ~6.0. An intracellular pH of ~7.0 has been reported in cancer cells[16–18]. The chemical shifts and coupling constants, used for MRS data analysis in the present study, were measured at pH 7.0 (ref. 10). As the proton NMR spectrum of 2HG is close to constant between pH 6.5–7.5 (**Supplementary Fig. 4**), the efficiency of detecting 2HG in gliomas should not be sensitive to tumor pH.

A PRESS sequence used for 2HG measurement in the present study is commonly available in clinical magnetic resonance systems. The field strength used here, 3 T, is becoming more commonly used in the academic and clinical magnetic resonance community, and the data-acquisition method could be implemented on standard hardware already in place in many magnetic resonance imaging centers. Without the need for more specialized instrumentation or the production of expensive exogenous probes, the detection of 2HG by MRS is a method that could

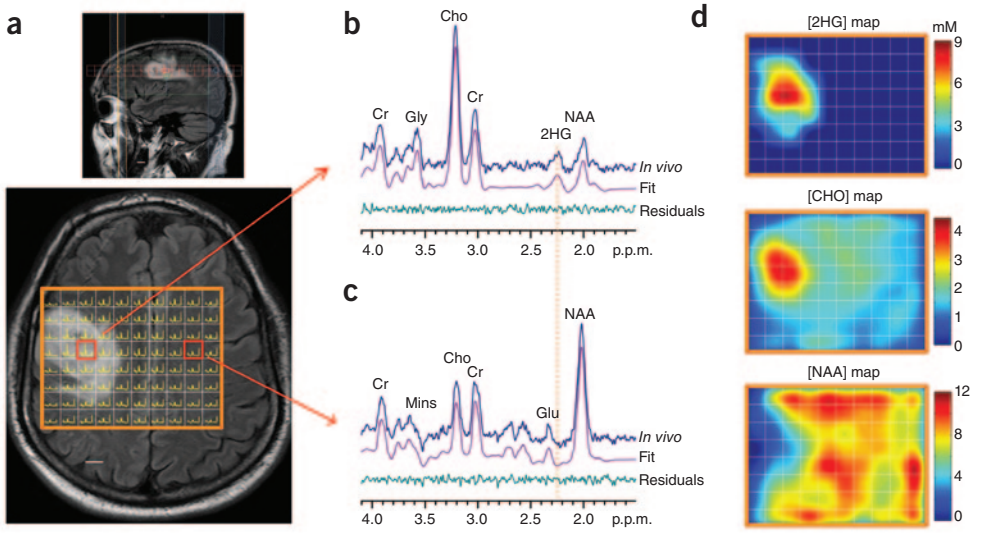

Figure 4 Spectroscopic imaging of 2HG. (**a**) Multivoxel imaging spectra from a subject with a WHO grade 3 oligodendroglioma are overlaid on the T_2w-FLAIR image. The grid size is 1 × 1 cm, with slice thickness 1.5 cm. The spectra are displayed between 4.1 p.p.m. and 1.8 p.p.m. (left to right). (**b**,**c**) Two representative spectra (one from the tumor and another from the contralateral normal brain) are shown together with LCModel fits and residuals. Mins, myoinositol. (**d**) The estimated concentrations of 2HG, choline and NAA in individual voxels were color coded for comparison. The NAA level in gray matter in normal brain was assumed to be 12 mM. Scale bars, 1 cm.

be quickly adopted for clinical use. As the presence of an *IDH1* or *IDH2* mutation makes the diagnosis of glioma when evaluating a brain mass, the ability to detect 2HG by MRS will be a valuable diagnostic tool. Although not obviating the need for a surgical procedure to determine tumor grade, the presence of 2HG on MRS would differentiate a tumor from a non-neoplastic process such as demyelinating disease. Moreover, the association of *IDH1* and *IDH2* mutations with improved survival among gliomas makes the detection of 2HG an important prognostic marker as well.

The additional clinical value of this biomarker may be in its dynamic measurement over the time course of treatment and follow up. If 2HG concentrations reflect changes in tumor cellularity, then proliferation would lead to increased 2HG concentrations, and tumor cells killed by radiation or chemotherapy would lead to decreased 2HG concentrations. Stable disease would be expected to have stable 2HG concentrations. Although these correlations are still speculative, potential clinical applications include the follow up of patients with WHO grade 2 gliomas who typically have a long period of minimal progression that is followed rapidly by aggressive growth and transformation to high grade. Similarly, the availability of an imaging biomarker to follow for the detection of recurrent disease or response to chemotherapy would be a major advance in the clinical management of patients with gliomas. Additional studies of the dynamic properties of 2HG measurement will address these potential uses.

METHODS

Methods and any associated references are available in the online version of the paper at http://www.nature.com/nm/.

Note: Supplementary information is available on the Nature Medicine website.

ACKNOWLEDGMENTS

This work was supported by US National Institutes of Health grants RC1NS0760675, R21CA159128, and RR02584 and by the Cancer Prevention Research Institute of Texas grant RP101243-P04. We thank C. Sheppard for expert management of the patient database and for coordinating research scans and tissue samples; S. McNeil for expert human subject care during scanning; C. Foong for expert assistance with pathological analysis of tumor; and R.L. Boriack for expert assistance with 2HG measurements by mass spectrometry.

AUTHOR CONTRIBUTIONS

C.C. developed the MRS methodology for 2HG detection, designed and performed the magnetic resonance experiments and data analysis, supervised the MRS study, prepared figures and wrote the manuscript. E.A.M. led all aspects of the human study, contributed to data analysis, preparation of the figures and writing of the manuscript. S.K.G. carried out magnetic resonance data acquisition and contributed to data analysis. D.R. performed mass spectrometry analysis on resected tumors and contributed to manuscript preparation. Z.K. synthesized 2HG and prepared a figure. R.J.D. and C.R.M. contributed to the conceptual approach, review of the data and manuscript preparation. K.J.H. and J.M.R. contributed to tumor sample collection and validation, neuropathological evaluation and diagnosis, evaluation of immunohistochemical stains and manuscript preparation. X.-L.Y. and T.M. performed the tissue evaluation of *IDH* mutations. I.M.-V. and J.M.P. contributed to conceptual analysis. B.E.M. recruited subjects and contributed to clinical data analysis and manuscript preparation. C.J.M. recruited subjects and contributed to manuscript preparation. R.M.B. contributed to the conceptual approach, led the tumor analysis workup, and contributed to data analysis and manuscript preparation.

COMPETING FINANCIAL INTERESTS

The authors declare no competing financial interests.

Published online at http://www.nature.com/naturemedicine/.
Reprints and permissions information is available online at http://www.nature.com/reprints/index.html.

1. Balss, J. *et al.* Analysis of the *IDH1* codon 132 mutation in brain tumors. *Acta Neuropathol.* **116**, 597–602 (2008).
2. Yan, H. *et al. IDH1* and *IDH2* mutations in gliomas. *N. Engl. J. Med.* **360**, 765–773 (2009).
3. Dang, L. *et al.* Cancer-associated IDH1 mutations produce 2-hydroxyglutarate. *Nature* **462**, 739–744 (2009).
4. Figueroa, M.E. *et al.* Leukemic *IDH1* and *IDH2* mutations result in a hypermethylation phenotype, disrupt TET2 function, and impair hematopoietic differentiation. *Cancer Cell* **18**, 553–567 (2010).
5. Christensen, B.C. *et al.* DNA methylation, isocitrate dehydrogenase mutation, and survival in glioma. *J. Natl. Cancer Inst.* **103**, 143–153 (2011).
6. Parsons, D.W. *et al.* An integrated genomic analysis of human glioblastoma multiforme. *Science* **321**, 1807–1812 (2008).
7. von Deimling, A., Korshunov, A. & Hartmann, C. The next generation of glioma biomarkers: *MGMT* methylation, *BRAF* fusions and *IDH1* mutations. *Brain Pathol.* **21**, 74–87 (2011).
8. Bottomley, P.A. Selective volume method for performing localized NMR spectroscopy. US Patent 4,480,228 (1984).
9. Mescher, M., Merkle, H., Kirsch, J., Garwood, M. & Gruetter, R. Simultaneous *in vivo* spectral editing and water suppression. *NMR Biomed.* **11**, 266–272 (1998).
10. Bal, D. & Gryff-Keller, A. ^{1}H and ^{13}C NMR study of 2-hydroxyglutaric acid and lactone. *Magn. Reson. Chem.* **40**, 533–536 (2002).
11. Krawczyk, H. & Gradowska, W. Characterisation of the ^{1}H and ^{13}C NMR spectra of N-acetylaspartylglutamate and its detection in urine from patients with Canavan disease. *J. Pharm. Biomed. Anal.* **31**, 455–463 (2003).
12. Govindaraju, V., Young, K. & Maudsley, A.A. Proton NMR chemical shifts and coupling constants for brain metabolites. *NMR Biomed.* **13**, 129–153 (2000).
13. Ernst, R.R., Bodenhausen, G. & Wokaun, A. *Principles of nuclear magnetic resonance in one and two dimensions* Ch. 2 (Clarendon Press, Oxford, UK, 1987).
14. Thompson, R.B. & Allen, P.S. Sources of variability in the response of coupled spins to the PRESS sequence and their potential impact on metabolite quantification. *Magn. Reson. Med.* **41**, 1162–1169 (1999).
15. Choi, C. *et al.* Improvement of resolution for brain coupled metabolites by optimized ^{1}H MRS at 7T. *NMR Biomed.* **23**, 1044–1052 (2010).
16. Gillies, R.J., Raghunand, N., Garcia-Martin, M.L. & Gatenby, R.A. pH imaging. A review of pH measurement methods and applications in cancers. *IEEE Eng. Med. Biol. Mag.* **23**, 57–64 (2004).
17. Griffiths, J.R. Are cancer cells acidic? *Br. J. Cancer* **64**, 425–427 (1991).
18. McLean, L.A., Roscoe, J., Jorgensen, N.K., Gorin, F.A. & Cala, P.M. Malignant gliomas display altered pH regulation by NHE1 compared with nontransformed astrocytes. *Am. J. Physiol. Cell Physiol.* **278**, C676–C688 (2000).
19. Provencher, S.W. Estimation of metabolite concentrations from localized *in vivo* proton NMR spectra. *Magn. Reson. Med.* **30**, 672–679 (1993).
20. Mlynárik, V., Gruber, S. & Moser, E. Proton T (1) and T (2) relaxation times of human brain metabolites at 3 tesla. *NMR Biomed.* **14**, 325–331 (2001).
21. Träber, F., Block, W., Lamerichs, R., Gieseke, J. & Schild, H.H. ^{1}H metabolite relaxation times at 3.0 tesla: measurements of T1 and T2 values in normal brain and determination of regional differences in transverse relaxation. *J. Magn. Reson. Imaging* **19**, 537–545 (2004).
22. Ganji, S.K. *et al.* T2 measurement of J-coupled metabolites in the human brain at 3T. *NMR Biomed.* published online, doi:10.1002/nbm.1767 (15 August 2011).
23. Norton, W.T., Poduslo, S.E. & Suzuki, K. Subacute sclerosing leukoencephalitis. II. Chemical studies including abnormal myelin and an abnormal ganglioside pattern. *J. Neuropathol. Exp. Neurol.* **25**, 582–597 (1966).
24. Keevil, S.F. *et al.* Absolute metabolite quantification by *in vivo* NMR spectroscopy: II. A multicentre trial of protocols for *in vivo* localised proton studies of human brain. *Magn. Reson. Imaging* **16**, 1093–1106 (1998).
25. Tong, Z., Yamaki, T., Harada, K. & Houkin, K. *In vivo* quantification of the metabolites in normal brain and brain tumors by proton MR spectroscopy using water as an internal standard. *Magn. Reson. Imaging* **22**, 1017–1024 (2004).
26. Sener, R.N. L-2 hydroxyglutaric aciduria: proton magnetic resonance spectroscopy and diffusion magnetic resonance imaging findings. *J. Comput. Assist. Tomogr.* **27**, 38–43 (2003).
27. Goffette, S.M. *et al.* L-2-Hydroxyglutaric aciduria: clinical, genetic, and brain MRI characteristics in two adult sisters. *Eur. J. Neurol.* **13**, 499–504 (2006).

ONLINE METHODS

Subject inclusion. We selected subjects from two University of Texas Southwestern Medical Center (UTSW) Institutional Review Board–approved brain tumor clinical protocols that have magnetic resonance imaging and include MRS as part of the study procedures. We obtained informed consent for each subject. Scans from 53 subjects were screened and were included for analysis of 2HG if (i) there was a visible tumor mass by standard magnetic resonance sequences (gadolinium enhancement or T_2w-FLAIR signal abnormality), (ii) MRS had been performed in at least 1 voxel in the tumor that was of acceptable spectral quality (singlet line width <6 Hz), and (iii) there was adequate tissue available for *IDH* gene sequencing. Scans from 30 subjects met these criteria, and 29 subjects had been imaged before initial surgery or after a limited surgical procedure (biopsy or subtotal resection) and had not been treated with chemotherapy or radiation. One subject with secondary GBM was imaged at the time of recurrence, 3 years after treatment with radiation. A search was done in each case for the availability of frozen tissue. In 13 of 30 cases, a frozen tumor sample was identified, with three cases having both tumor and a sample of adjacent, non–tumor-bearing brain available for analysis.

Magnetic resonance spectroscopy data acquisition. Experiments were carried out on a 3-T whole-body scanner (Philips Medical Systems). A body coil was used for radiofrequency transmission and an eight-channel head coil was used for reception. Data were acquired according to our published methods[28]. PRESS[8] and scalar difference editing[9] were used for measuring 2HG in brain tumors. For editing, two 20-ms Gaussian 180° pulses, tuned to 1.9 p.p.m., were switched on and off in alternate scans to generate an edited H2 signal at 4.02 p.p.m. in difference spectra. The echo times of PRESS and editing were 97 ms and 106 ms, respectively. The quantum-mechanical simulations were carried out by means of the product operator–based transformation matrix algorithm (**Supplementary Methods**). For *in vivo* magnetic resonance scans, following the survey imaging, T_2w-FLAIR images were acquired to identify tumor regions. For single-voxel–localized data acquisition, a $2 \times 2 \times 2$ cm^3 voxel was positioned in the tumor mass. PRESS acquisition parameters included a sweep width of 2500 Hz, 2,048 sampling points, a repetition time of 2 s, and 64 averages (scan time 2.1 min). Editing data were acquired with 384 averages (scan time 13 min). An unsuppressed water signal was acquired with an echo time of 14 ms and a repetition time of 20 s for use as a reference in metabolite quantification. Spectroscopic imaging data were acquired, using the optimized PRESS echo time, from a slice 1.5 cm thick with a resolution of 1×1 cm^2. We carried out undersampling of k-space data by 20%, the scan time being approximately10 min (two averages, repetition time = 1.3 s). Data were zero filled for the unacquired k-space points and filtered with a cosine function before Fourier transformation.

Magnetic resonance spectroscopy data analysis. Data were analyzed as described[28]. Following a 1-Hz apodization, spectra were fitted with LCModel software[19], using calculated spectra of 20 metabolites as basis functions. The basis set included spectra of 2HG, NAA, GABA, glutamate, glycine, creatine, myoinositol, glutamine, lactate, alanine, acetate, aspartate, ethanolamine, glutathione, phosphorylethanolamine, *scyllo*-inositol, taurine, *N*-acetylaspartylglutamate, glucose and choline. The metabolite concentrations were estimated with respect to the short-echo-time water signal. Assuming an equal composition of gray and white matter in tumors, we used a water concentration value of 42.3 M, calculated from the literature values[23] for the water concentrations in gray and white matter. Relaxation effects on metabolite signals were corrected using published metabolite T_2 and T_1: T_2 = 150 ms, 230 ms and 280 ms for Cr, Cho and NAA, and 180 ms for other metabolites, respectively; T_1 = 1.2 ms for 2HG, glutamate, glutamine and myo-inositol, and 1.5 ms for other metabolites[20–22].

Immunohistochemistry for detection of the R132H mutation in *IDH1*. Paraffin sections were cut at 4-μm thickness and prepared according to standard clinical methods. The primary antibody for *IDH1* R132H (Dianova) was diluted 1 in 20.

***IDH1* and *IDH2* DNA sequencing.** DNA was prepared from frozen tissue by standard methods or from formalin-fixed paraffin embedded samples according to a published method[29]. Primers for *IDH1* and *IDH2* sequencing were used according to published methods[1,3].

Measurement of 2HG enantiomers by mass spectrometry. D-2HG and L-2HG were extracted from tumor tissue and normal brain, and LC-MS/MS analyses were performed as described[30,31].

Statistical analyses. Cramér-Rao lower bounds of metabolite estimates, which represent the lower bounds of the precision, were obtained with the built-in algorithm of the LCModel software[19].

Additional methods. Detailed methodology for 2HG synthesis and transformation matrix–incorporated density-matrix simulations is described in the **Supplementary Methods**.

28. Choi, C. *et al.* Measurement of glycine in the human brain *in vivo* by ^{1}H-MRS at 3 T: application in brain tumors. *Magn. Reson. Med.* **66**, 609–618 (2011).
29. Maher, E.A. *et al.* Marked genomic differences characterize primary and secondary glioblastoma subtypes and identify two distinct molecular and clinical secondary glioblastoma entities. *Cancer Res.* **66**, 11502–11513 (2006).
30. Rakheja, D., Mitui, M., Boriack, R.L. & DeBerardinis, R.J. Isocitrate dehydrogenase 1/2 mutational analyses and 2-hydroxyglutarate measurements in Wilms tumors. *Pediatr. Blood Cancer* **56**, 379–383 (2011).
31. Rakheja, D. *et al.* Papillary thyroid carcinoma shows elevated levels of 2-hydroxyglutarate. *Tumour Biol.* **32**, 325–333 (2011).

doi:10.1038/nm.2682

CORRECTION NOTICE

Nat. Med.; **doi:10.1038/nm.2682**

2-hydroxyglutarate detection by magnetic resonance spectroscopy in subjects with *IDH*-mutated gliomas

Changho Choi, Sandeep K Ganji, Ralph J DeBerardinis, Kimmo J Hatanpaa, Dinesh Rakheja, Zoltan Kovacs, Xiao-Li Yang, Tomoyuki Mashimo, Jack M Raisanen, Isaac Marin-Valencia, Juan M Pascual, Christopher J Madden, Bruce E Mickey, Craig M Malloy, Robert M Bachoo & Elizabeth A Maher

In the version of this supplementary file originally posted online, the equations [4], [5], [6] and [8] were incorrect. The error has been corrected in this file as of 31 January 2012.

SUPPLEMENTARY FIGURES

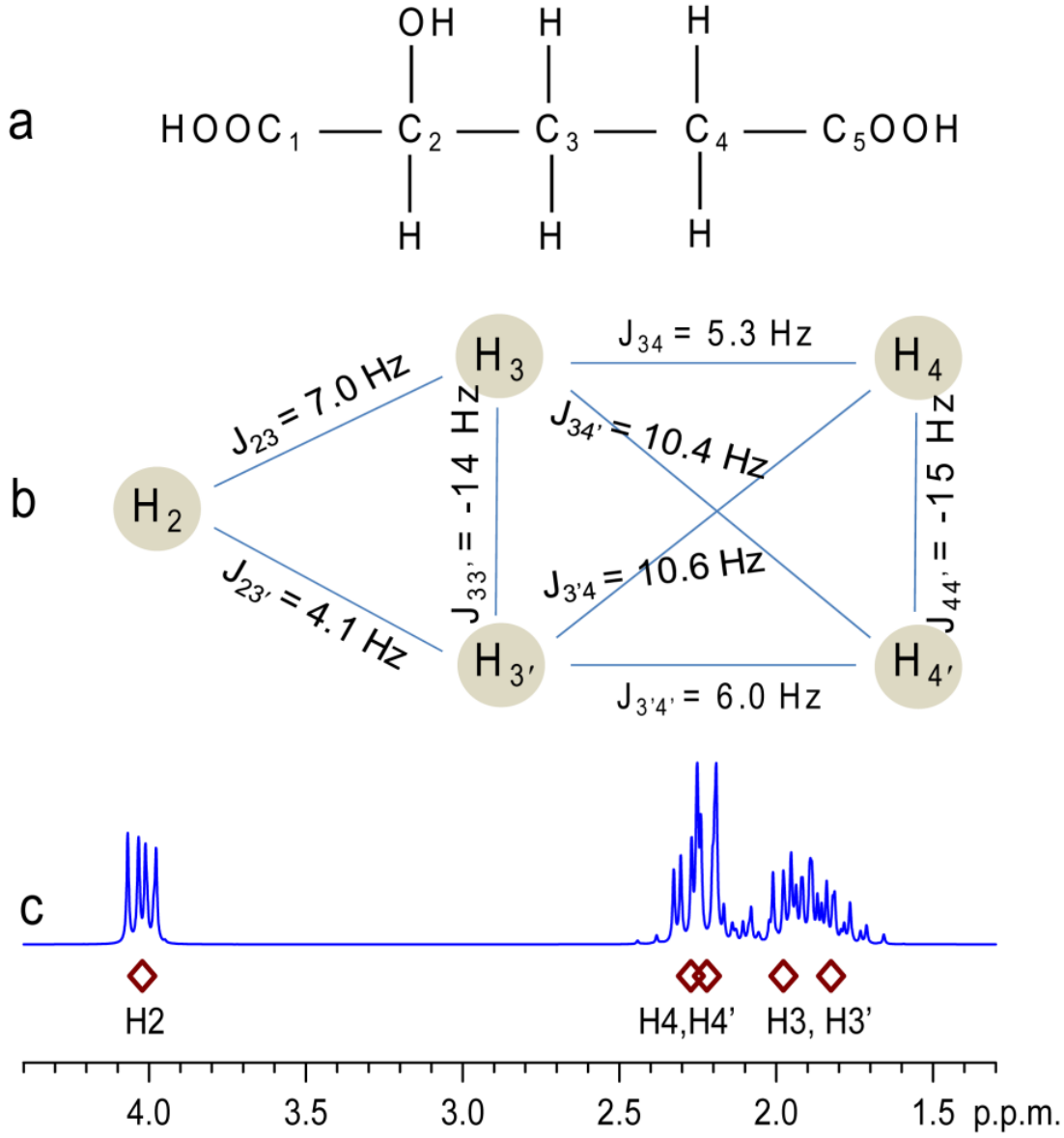

Supplementary Figure 1. NMR characteristics of 2HG. (**a**) Molecular structure of 2HG. The non-exchangeable protons of C2, C3 and C4 are detectable in ^{1}H MRS. (**b**) Scalar coupling connections between the non-exchangeable protons. (**c**) A ^{1}H MR spectrum of 2HG calculated for single-pulse acquisition at 3T is shown together with the spectral locations of the H2, H3 and

H4 spin resonances. The calculated time-domain signal was multiplied by a 1-Hz exponential function before Fourier transformation.

Nature Medicine doi:10.1038/nm.2682

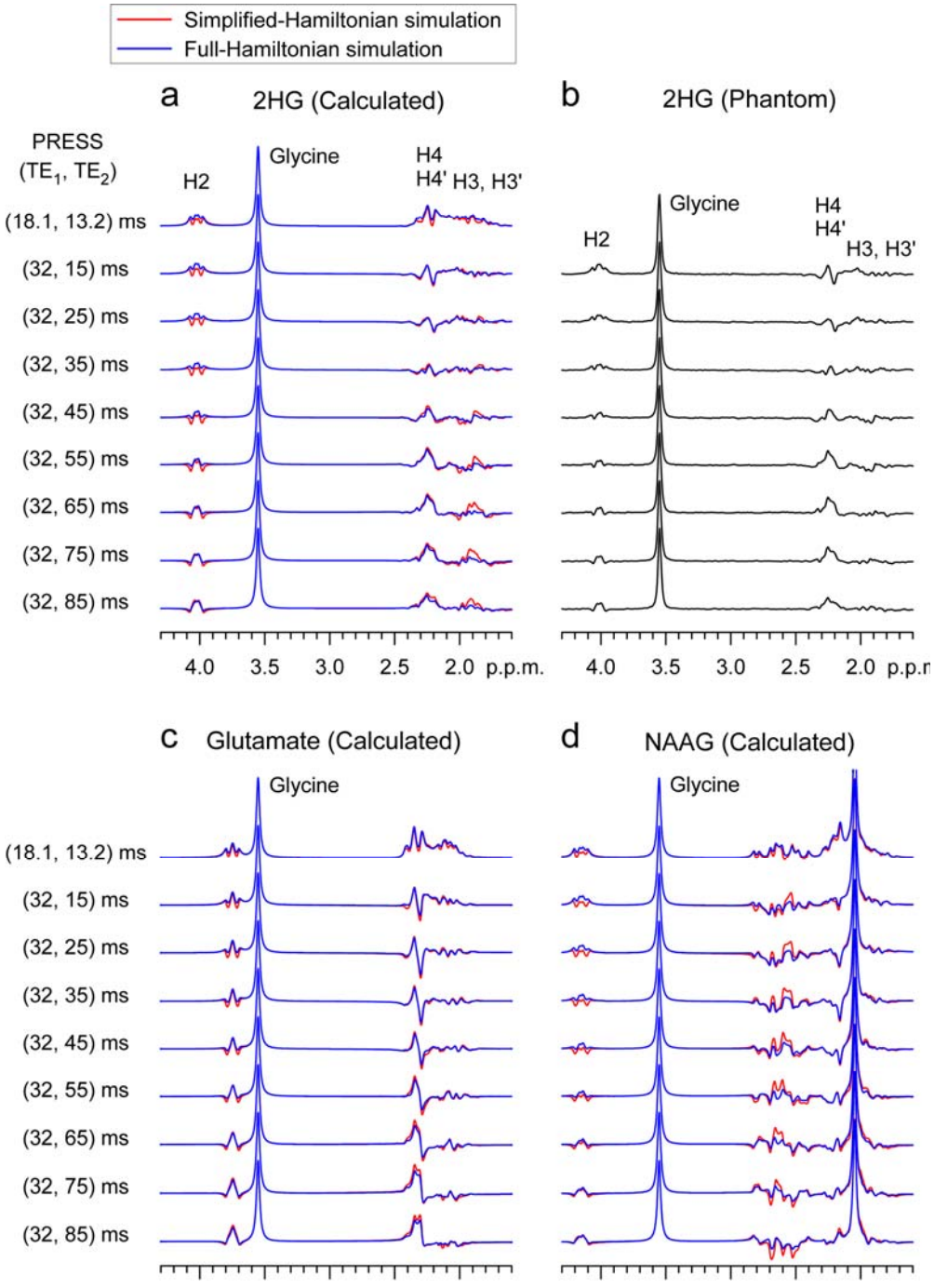

Supplementary Figure 2. (**a,b**) Comparison of PRESS 2HG spectra calculated with full-Hamiltonian model (shaped slice-selective radio-frequency pulses used for *in vivo*) and with simplified-Hamiltonian model (1-μs non-selective radio-frequency pulses) for various PRESS

Nature Medicine doi:10.1038/nm.2682

subecho time pairs (TE1, TE2). Spectra, calculated for [2HG]/[Gly] = 1, are scaled with respect to the Gly singlet at 3.55 p.p.m. in each spectrum. The 2HG spectral pattern and signal intensities differ between the models, largely due to the finite bandwidth of the slice-selective 180° RF pulses and the coherence proliferation during the radio-frequency pulses. For short echo times (echo time = TE1+TE2 < 70 ms), the H4 and H3 signals are similar, and the H2 multiplet is different between the models. As echo time increases, the discrepancy between the H3 multiplets from the two models becomes substantial. The difference in the H4 multiplet is noticeable at long echo times. This result indicates that the full Hamiltonian model should be used for optimizing the MRS sequences and creating basis spectra for spectral fitting. (**c,d**) Similarly, calculated spectra of glutamate (c) and N-acetylaspartylglutamate (NAAG) (d) show discrepancy between the simplified- and full-Hamiltonian models. NAAG exhibits substantial differences between the models due to the relatively large spectral distances between the coupling partners (i.e., ~2.6 and 4.6 p.p.m. of aspartyl moiety, and 1.9 and 4.15 p.p.m. of glutamate moiety). Spectra in a, c, and d were calculated for an identical concentration, ignoring T1 and T2 relaxation effects. Calculated and phantom spectra were all broadened to singlet linewidth of 4 Hz.

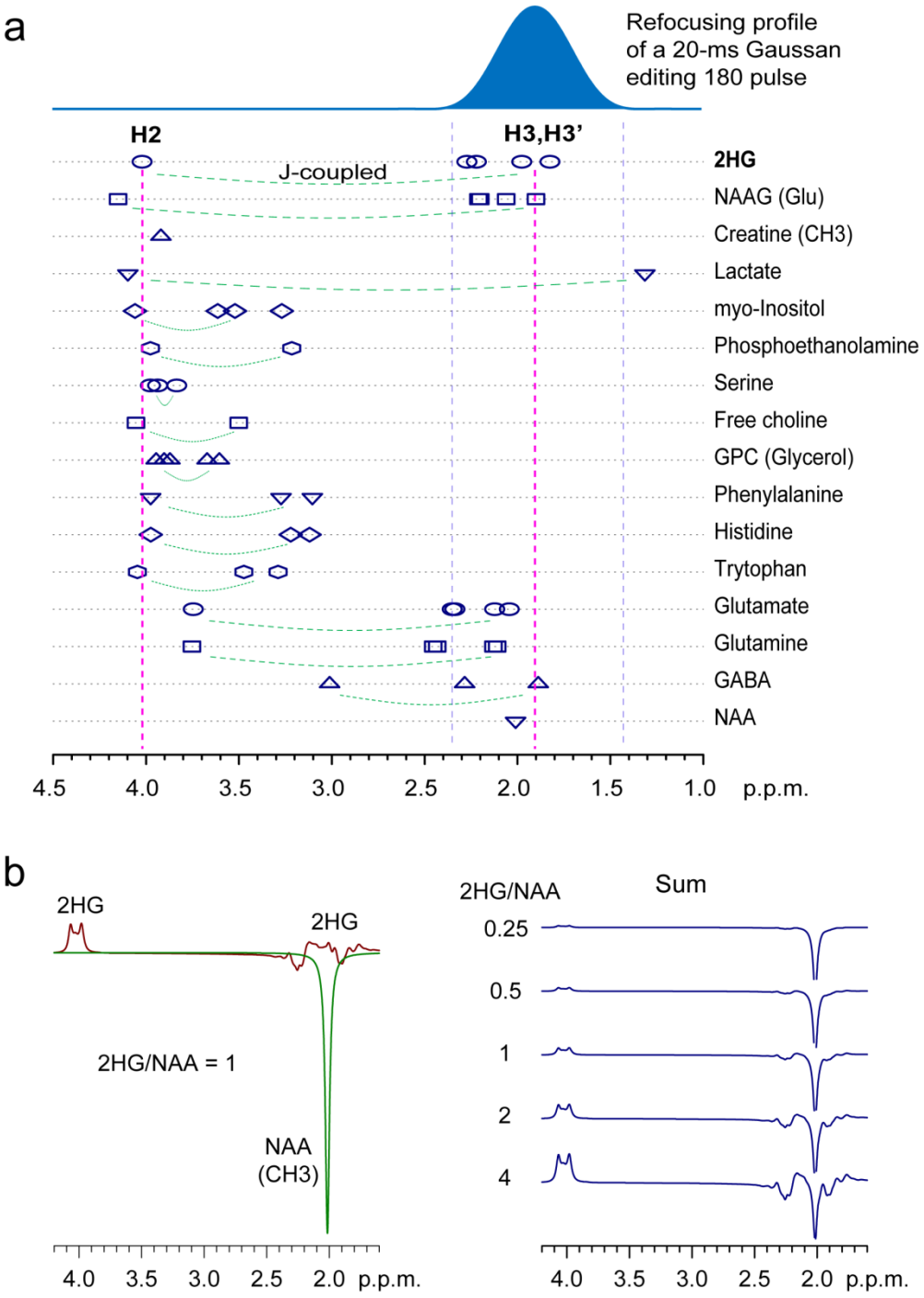

Supplementary Figure 3. (**a**) The refocusing profile of the 20-ms Gaussian 180° radio-frequency pulse (truncated at 12%; bandwidth = 56 Hz) used for difference editing is shown together with the ^{1}H resonances of 2HG and metabolites that have resonances in the proximity of

the 2HG H2 resonance at 4.02 p.p.m., and those of metabolites which are co-edited. Green (dashed) lines indicate scalar coupling connections of metabolite resonances. The editing 180° pulse (E180) is tuned to 1.9 p.p.m. to selectively rotate the 2HG H3 spins through 180° in a subscan (E180-on). An edited 2HG H2-spin signal at 4.02 p.p.m. is obtained *via* subtraction between this subspectrum and an E180-off subspectrum. The 4.15 p.p.m. resonance of the glutamate moiety of NAAG, that has coupling partners at ~1.9 p.p.m., is coedited. However, the coedited NAAG signal may not interfere with 2HG detection substantially since the coedited resonance is fairly separated (by 0.13 p.p.m.) from the 2HG H2 resonance (4.02 p.p.m.). In practice, a noticeable coedited signal at 4.15 p.p.m. was not detected *in-vivo* due to the relatively low concentrations of NAAG in brain. The 3.92 p.p.m. singlet of creatine is identical in subspectra, so canceled *via* subtraction. Lactate has a resonance at 4.1 p.p.m. which is coupled to the 1.31 p.p.m. resonance. This resonance is not affected by the E180, thus the lactate 4.1 p.p.m. resonance is not coedited. There are several additional coupled resonances in the proximity of the 2HG H2 resonance, but these resonances are canceled *via* subtraction since their coupling partners are not influenced by the editing 180° pulse. Glutamate, glutamine, GABA and NAA have resonances at ~1.9 p.p.m. and the resulting non-zero signals at 1.8 - 2.3 p.p.m. overlap with the 2HG H4 and H3 multiplets in the difference spectra. However, since the edited 2HG H2 signal uniquely appears at 4.02 p.p.m., the signal overlaps at 1.8 - 2.3 p.p.m. do not interfere with 2HG estimation considerably. (**b**) Calculated edited spectra of 2HG and NAA for equal concentrations (left) are illustrated together with sum spectra at 2HG-to-NAA concentration ratios of 0.25, 0.5, 1, 2, and 4 (right).

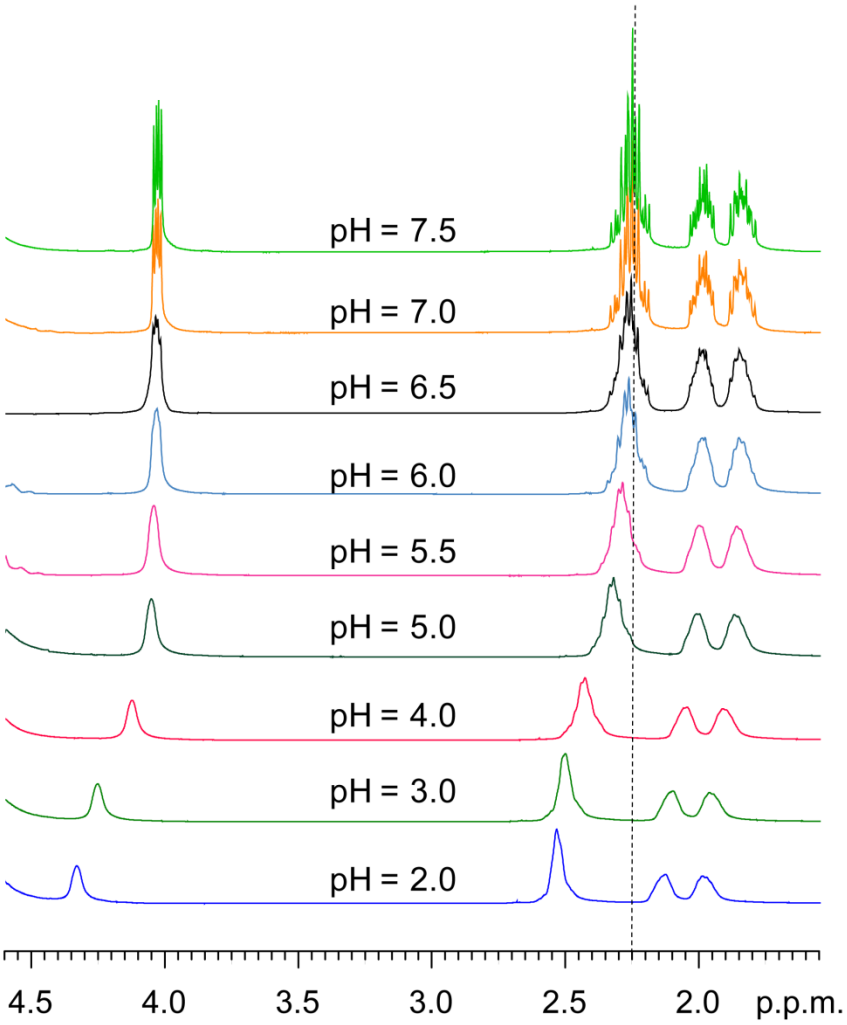

Supplementary Figure 4. The pH dependence of the ^{1}H NMR spectrum of 2HG in D_2O at 298 K and 9.4 T. Each spectrum was recorded after adjusting the pH of sodium 2-HG with DCl to the desired pH (7.5 - 2.0). The free induction decay was acquired following a standard single pulse excitation. Each spectrum was recorded with an internal standard of *tert*-butanol (1.24 p.p.m.) whose resonance does not depend on pH. A vertical dotted line is drawn at 2.25 p.p.m..

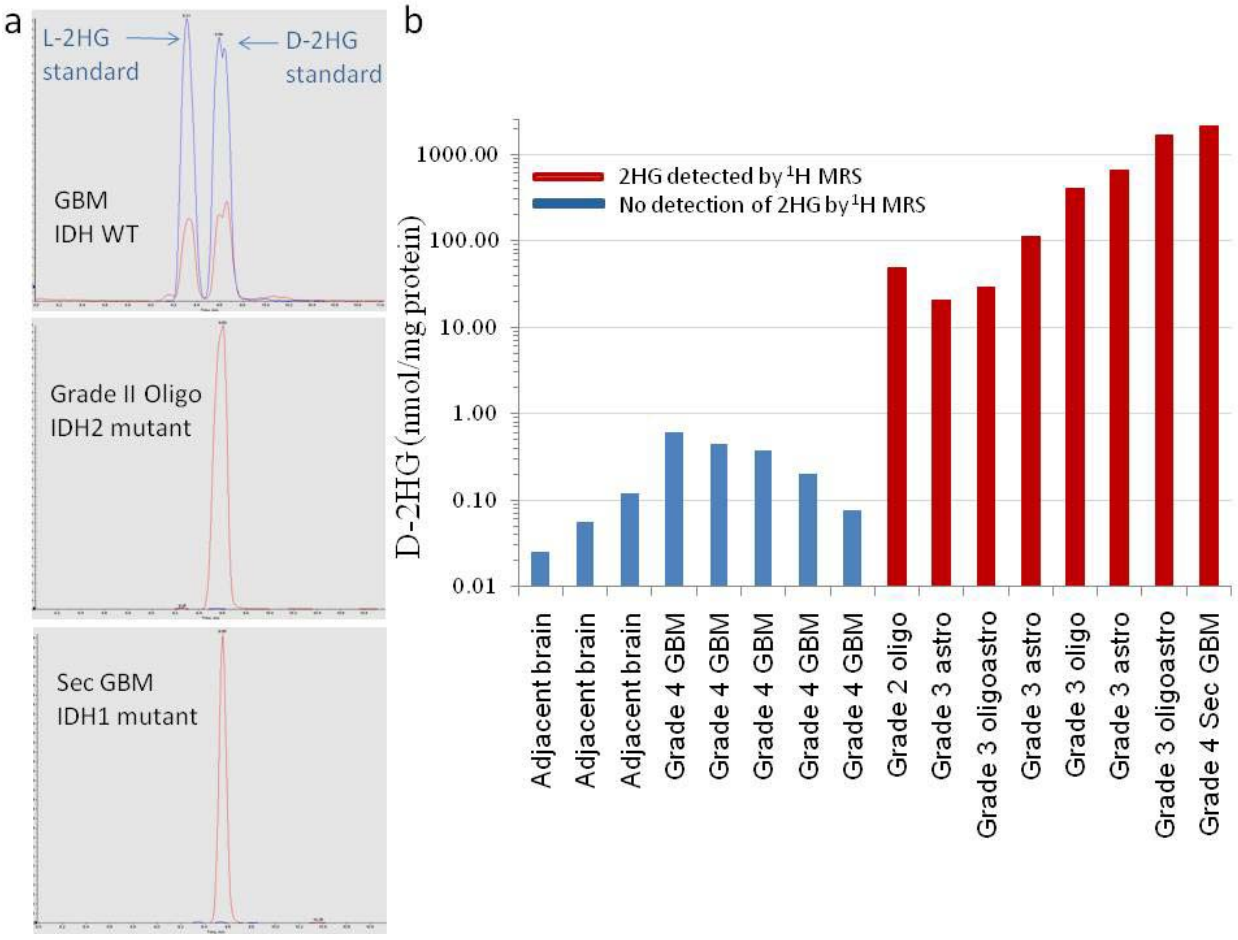

Supplementary Figure 5. Measurement of 2HG in tissue samples. (**a**) Tracings from liquid chromatography/tandem mass spectroscopy of 2HG in 3 patients (red peaks). Upper panel: blue peaks represent labeled internal standards for L-2HG and D-2HG. GBM with wild type IDH show similar levels of L- and D-2HG. Grade 2 oligodendroglioma (middle panel) and secondary GBM (lower panel), samples diluted 10 fold, demonstrate markedly elevated levels of D-2HG. (**b**) D-2HG levels in 3 tissue samples of brain adjacent to tumor and 13 tumor samples. Red bars: patients who had measurable 2HG by MRS. Blue bars: patients without detectable 2HG by MRS.

Nature Medicine doi:10.1038/nm.2682

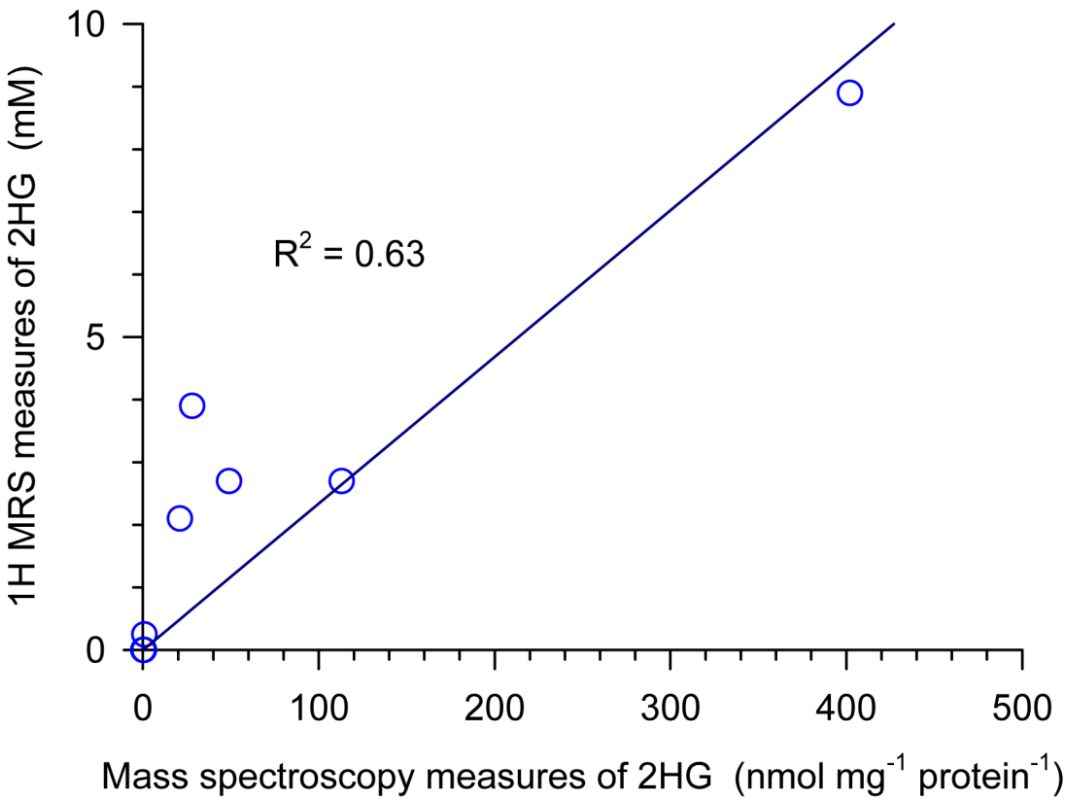

Supplementary Figure 6. **L**inear regression of ^{1}H MRS estimates of 2HG concentration *vs*. mass spectrometry measures of 2HG. The coefficient of determination (R^2) was 0.63. The MRS and mass spectrometry data obtained at different time points (specified with asterisks in Supplementary Table 1) are not included.

SUPPLEMENTARY TABLE

Histological Diagnosis	2HG (MRS) mM (CRLB)	D-2HG nmol/mg prot	L-2HG nmol/mg prot	*IDH1*	*IDH2*
Oligodendroglioma (WHO Grade 2)	2.7 (13%)	48.68	0.12	WT	mutant
Astrocytoma (WHO Grade 3)	2.1 (16%)	20.61	0.47	mutant	WT
Astrocytoma (WHO Grade 3)	2.7 (11%)	113.39	0.17	WT	mutant
Oligoastrocytoma (WHO Grade 3)	3.9 (6%)	28.41	0.21	mutant	WT
Oligodendroglioma (WHO Grade 3)	8.9 (3%)	401.79	0.79	mutant	WT
Oligoastrocytoma (WHO Grade 3)	3.4 (8%)*	1673.50	0.05	WT	mutant
Sec Glioblastoma (WHO Grade 4)	2.1 (15%)*	2118.10	0.23	mutant	WT
Glioblastoma (WHO Grade 4)	Not Detected	0.14	0.07	WT	WT
Glioblastoma (WHO Grade 4)	Not Detected	0.20	0.17	WT	WT
Glioblastoma (WHO Grade 4)	Not Detected	0.38	0.36	WT	WT
Glioblastoma (WHO Grade 4)	Not Detected	0.44	0.29	WT	WT
Glioblastoma (WHO Grade 4)	Not Detected	0.61	0.19	WT	WT
Glioblastoma (WHO Grade 4)	Not Detected	0.84	0.77	WT	WT

Supplementary Table 1: Correlation between 2HG concentration measured by MRS (PRESS) and tissue levels of D- and L-2HG by liquid chromatography-tandem mass spectrometry. The symbol * refers to patients whose first scans to evaluate 2HG were done at the time of tumor recurrence, >2 years after the time of the initial tumor resection. The remainder of the patients had the initial scan to evaluate 2HG at the time of the initial surgical resection. Abbreviation: WT – wild type.

Nature Medicine doi:10.1038/nm.2682

Supplementary Methods

Synthesis of disodium salt of 2-hydroxyglutarate:

Disodium salt of 2-hydroxyglutarate was in-house synthesized and used for making a 2HG phantom (pH = 7.0) for validating the MRS methods. (S)-(+)-5-Oxo-2-tetrahydrofurancarboxylic acid (500 mg, Aldrich) was dissolved in water (2 mL) and two equivalents of sodium hydroxide solution (2M, 3.84 mL) were added. The mixture was stirred at room temperature overnight and then lyophilized to produce a quantitative yield of the disodium salt of 2-hydroxyglutarate.

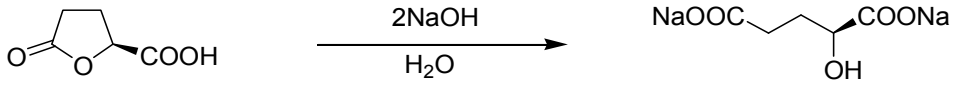

Quantum-mechanical simulations by the product-operator-based transformation matrix algorithm:

Quantum-mechanical simulations were carried out to optimize the echo times of the PRESS and difference editing for 2HG measurement and to create the model spectra of metabolites for LCModel spectral fitting. The time evolution of the density operator was calculated numerically incorporating the shaped 90° and 180° radio-frequency and gradient pulses. The product-operator-based transformation matrix method [1,2] was employed to calculate the spectra at numerous echo times. An echo time that gives maximum 2HG signal was then selected for each sequence and applied in the patient study. The density matrix simulations were programmed with Matlab (The MathWorks Inc.). Published chemical shift and coupling constants were used in the simulation [3-5].

The time evolution of the density operator ρ is described by the Liouville-von Neumann equation [1]

$$\partial\rho/\partial t = -i\,[H, \rho], \qquad [1]$$

which has a solution

$$\rho = exp(-iHt)\ \rho_0\ exp(iHt), \qquad [2]$$

for a time-independent Hamiltonian H. The Hamiltonian H may include the chemical shift (CS) and scalar coupling (J) terms and the radio-frequency (RF) and gradient (G) pulse terms,

$$H = H_{CS} + H_J + H_{RF} + H_G, \qquad [3]$$

in the rotating frame.

For a spin system with N coupled protons (spin = 1/2), 4^N product operators (PO) can constitute a complete set in Liouville space [6]. The density matrix ρ may be written as a linear sum of the PO terms α,

$$\rho = \sum_{i=1}^{4^N} c_i \alpha_i\ , \qquad [4]$$

where ρ and α are $2^N \times 2^N$ square matrices with complex entries, and the coefficient c is real. The density operator can be expressed as a column vector σ which is composed of the coefficients c,

$$\sigma = \begin{pmatrix} c_1 \\ c_2 \\ \vdots \\ c_{4^N} \end{pmatrix}. \qquad [5]$$

The density operator evolution during an radio-frequency pulse can be put in terms of a single matrix multiplication [1],

$$\sigma' = \begin{pmatrix} c_1' \\ c_2' \\ \vdots \\ c_{4^N}' \end{pmatrix} = \begin{pmatrix} T_{1,1} & T_{1,2} & \cdots & T_{1,4^N} \\ T_{2,1} & T_{2,2} & \cdots & T_{2,4^N} \\ \vdots & \vdots & \cdots & \vdots \\ T_{4^N,1} & T_{4^N,2} & \cdots & T_{4^N,4^N} \end{pmatrix} \begin{pmatrix} c_1 \\ c_2 \\ \vdots \\ c_{4^N} \end{pmatrix} = T\,\sigma, \qquad [6]$$

where the transformation matrix T is a $4^N \times 4^N$ square matrix with real entries. The T-matrix was constructed for each spatially/spectrally-selective shaped radio-frequency pulse and used for

calculating the time evolution of the density operator during the MRS sequences for each metabolite.

For a time-dependent radio-frequency pulse whose envelope consists of n numbers as a function of time, H_{RF} and consequently H may be constant during each time period Δt. The density operator following the RF pulse was calculated using a (total) time evolution operator V_{total},

$$\rho = V_{total}^{-1}\, \rho_0\, V_{total}, \qquad [7]$$

where

$$V_{total} = V_1 V_2 \cdots V_i \cdots V_n . \qquad [8]$$

The time evolution operator for the i-th period of the radio-frequency pulse, V_i, was obtained using

$$V_i = U\ exp\,(-i\, H_i^{diag}\ \Delta t)\, U^{-1}, \qquad [9]$$

where H_i^{diag} (= $U^{-1}H_iU$) and U are the diagonalized matrix and the unitary matrix of the Hamiltonian of the i-th period, H_i, respectively.

When a gradient pulse was applied during an radio-frequency pulse for slice selection, since H_G and consequently H are position dependent, the space was divided into small segments and the calculation of Eq. [7] was undertaken for individual segments, assuming uniform H_G within each segment. The simulation for slice selection was conducted on a 20 mm thick slice at the center of a 30 mm sample. The sample space was divided into 150 segments, the spatial resolution being 1% with respect to the slice thickness (*i.e.*, 0.01 = 30/150/20). The 90° and 180° slice-selective radio-frequency pulse envelopes consisted of 500 and 200 digits for radio-frequency amplitude/phase variations, respectively. The bandwidths of the slice-selective 90° and 180° pulses were 4220 and 1260 Hz, respectively. With a radio-frequency carrier at 3

p.p.m., the slices of resonances between 1 – 5 p.p.m. were all included within the sample dimension for both 90° and 180° radio-frequency pulses. For the 180° pulse, two density matrices were calculated with two orthogonal radio-frequency phases (*i.e.*, 0 and $\pi/2$), and the slice-localized density matrix was obtained *via* subtraction between the matrices,

$$\rho_{slice} = (\rho_{\phi=0} - \rho_{\phi=\pi/2})/2. \quad [10]$$

The square matrix ρ_{slice} was then converted to a column vector σ, whose *i*-th element was calculated from

$$c_i = trace(\alpha_i \rho_{slice}), \quad [11]$$

where α_i is the normalized *i*-th PO term of the spin system and $i = 1, 2, \ldots, 4^N$. A single-column matrix was calculated from each PO term as an initial density operator prior to the radio-frequency pulse, and placed in the corresponding column of the *T*-matrix. For 2HG with 5 coupled spins, a $4^5 \times 4^5$ transformation matrix was constructed from the 4^5 column vectors, each from each PO term. The calculation of the *T*-matrix of 2HG for the slice selective 180° pulse was completed in ~7 hours in a PC. The *T*-matrix calculation time for the PRESS 90° RF pulse was relatively minimal (~1 min) because the calculation was to be done only for a single PO term (*i.e.*, I_z). For calculating a spectrum following a PRESS sequence

$$90 - TD_1 - 180 - TD_2 - 180 - TD_3 - \text{Acquisition}, \quad [12]$$

$$| \leftarrow \quad TE_1 \quad \rightarrow | \leftarrow \quad TE_2 \quad \rightarrow |$$

the simulation began with the calculated density matrix of the slice-selective 90° pulse. The time evolution during the inter-radio-frequency pulse delay (TD_1) was calculated using

$$\rho = V^{-1} \rho_0 V, \quad [13]$$

where $V = U\, exp(-i\, H^{diag}\, TD_1)\, U^{-1}$, and H^{diag} and U were formed from $H = H_{CS} + H_J$. After this, the square density ρ matrix was converted to a column matrix σ using Eq.[11] and multiplied by

the 180° pulse *T*-matrix (Eq. [6]), giving a column matrix at the end of the ss180. This column matrix was then converted to a square matrix ρ for calculating the density operator evolution during the subsequent time delay (TD_2). The calculation of the density operator evolution was continued to obtain the density operator ρ at the end of the sequence. The expectation values of single-quantum coherences were then extracted from the ρ, using $trace(I_{-}\rho)$, to construct a time-domain signal, which was Fourier transformed to obtain a spectrum in the frequency domain. The spoiling gradients symmetric about the PRESS 180° pulses were omitted in the simulation because the 2-step phase cycling in the *T*-matrix calculation eliminated the outer-band magnetization completely. With this transformation matrix method, a 3D-localized PRESS spectrum of 2HG was calculated in < 0.5 s in a PC.

For calculating a difference edited spectrum from a sequence scheme [7],

$$90 - 180 \quad - \text{ E180 } - 180 - \text{ E180} - \text{Acquisition} \qquad [14]$$

$$| \leftarrow TE_1 \rightarrow | \leftarrow \qquad TE_2 \qquad \rightarrow |$$

the density operator evolutions during the slice-selective 90° and 180° RF pulses and the inter-RF pulse delays were calculated similarly to the PRESS simulation. Two spectra were calculated; one with editing 180° pulses (E180) turned on (subscan-A) and another with E180 turned off (subscan-B). The spoiling gradient pulses were applied similarly to the published scheme [7]. Since the E180 pulses, tuned to 1.9 p.p.m., nullify the transverse components of the 2HG H3 spins, the *T*-matrix of the E180 was constructed from averaging over two density matrices obtained with RF phases 0 and π/2,

$$\rho_{E180} = (\rho_{\phi=0} + \rho_{\phi=\pi/2})/2. \qquad [15]$$

In the E180-on subscan, the coupling of the H3 spins to the H2 spin was decoupled, thereby leading to an inphase H2 multiplet. The E180-off subscan was essentially the same as PRESS.

A difference spectrum was obtained from the two subspectra, (A–B)/2. The Gaussian envelope of the E180 consisted of 500 numbers. The *T*-matrix calculation time for the 2HG 5-spin system was ~20 min. Using this *T*-matrix algorithm, a 3D-localized difference spectrum of 2HG was calculated in ~1 s.

Supplementary References

1. Ernst, R.R., Bodenhausen, G. & Wokaun, A. *Principles of nuclear magnetic resonance in one and two dimensions*, (Clarendon Press, Oxford, 1987).

2. Thompson, R.B. & Allen, P.S. Sources of variability in the response of coupled spins to the PRESS sequence and their potential impact on metabolite quantification. *Magn Reson Med* **41**, 1162-1169 (1999).

3. Fan, T.W.-M. Metabolite profiling by one- and two-dimensional NMR analysis of complex mixtures. *J Prog Nuc Magn Reson Spec* **28**, 161-219 (1996).

4. Govindaraju, V., Young, K. & Maudsley, A.A. Proton NMR chemical shifts and coupling constants for brain metabolites. *NMR Biomed* **13**, 129-153 (2000).

5. Bal, D. & Gryff-Keller, A. 1H and 13C NMR study of 2-hydroxyglutaric acid and its lactone. *Magn Reson Chem* **40**, 533-536 (2002).

6. Sorensen, O.W., Eich, G.W., Levitt, M.H., Bodenhausen, G. & Ernst, R.R. Product operator formalism for the description of NMR pulse experiments. *J Prog Nuc Magn Reson Spec* **16**, 163-192 (1983).

7. Mescher, M., Merkle, H., Kirsch, J., Garwood, M. & Gruetter, R. Simultaneous in vivo spectral editing and water suppression. *NMR Biomed* **11**, 266-272 (1998).